An Experimental and Numerical Study of Sound Propagation from a Supersonic Jet Passing through a Rigid-Walled Duct with a J-Deflector

Max Kandula[†]

Sierra Lobo, Inc., John F. Kennedy Space Center, FL 32988, USA

(Received 7 September 2005; revised 1 February 2006; accepted 10 April 2006)

The generation, propagation, and radiation of sound (the acoustical characteristics) from a perfectly expanded Mach 2.5 cold supersonic jet of 25.4 mm exit diameter flowing through an enclosed rigid-walled duct with an upstream J-deflector have been studied experimentally and numerically. In the experiments, the nozzle is mounted vertically, with the nozzle exit plane at a height of 73 jet diameters above ground level. Relative to the nozzle exit plane, the location of the duct inlet is varied at 10, 5, and –1 jet diameters. Far-field sound pressure levels were obtained at 54 jet diameters above ground with the aid of acoustical sensors equally spaced around a circular arc of radius equal to 80 jet diameters. Data on the acoustic field were obtained with and without the duct. The numerical simulations were carried out with the help of the OVERFLOW Navier-Stokes computational fluid dynamics (CFD) code in conjunction with a one-equation turbulence model. While the near-field sound sources were computed by the CFD code, the far-field sound was evaluated by the Kirchhoff surface integral formulation. Predictions of the far-field directivity of the overall sound pressure level (OASPL) agree satisfactorily with the experimental data. CFD calculations also suggest that there was significant entrainment of air into the duct, with the mass flow rate of entrained air being about three times the jet exit mass flow rate.

[†] Member of the International Institute of Acoustics and Vibration (IIAV)

Nomenclature

A	– amplitude of the disturbance
c	– sound velocity
d_j	– jet exit diameter
f	– frequency
h	– distance between nozzle exit plane (NEP) and the duct entrance
$\dot{m}$	– mass flow rate
$M = V/c$	– Mach number
p	– instantaneous pressure
p_m	– mean pressure
$p' = 2\frac{(p - p_m)}{\rho_\infty c_\infty^2}$	– dimensionless acoustic pressure disturbance
r	– distance from the sound source
r_j	– jet exit radius
$\mathrm{Re} = \rho_j u_j d_j / \mu_j$	– Reynolds number
$St = f d_j / u_j$	– Strouhal number
T	– temperature
u, v, w	– Cartesian velocity components
u', v', w'	– dimensionless velocity disturbance (scaled by c_∞)
$u^* = \sqrt{\tau_w/\rho}$	– friction velocity
V	– velocity
x, y, z	– Cartesian coordinates
$y^* = y u^*/\nu$	– dimensionless distance from the wall

Greek Symbols

μ	– dynamic viscosity
ρ	– density
$\nu = \mu/\rho$	– kinematic viscosity
τ_w	– wall shear stress
ω	– angular frequency of the disturbance

Subscripts

j	– jet
m	– time-mean
∞	– ambient fluid

1. INTRODUCTION

In recent years there has been considerable interest in the design of exhaust ducts for jet noise mitigation systems for launch vehicles devoid of water injection. Clean (dry) launch pads with ducted exhausts are preferable to those fitted with water deluge systems for sound suppression with regard to operational costs and the frequency of launches. Thus, the overall process of sound emission from partially ducted rocket exhausts is of great practical interest in the understanding of sound suppression systems for launch vehicles. Detailed knowledge of the behaviour of the sound radiation from these ducted exhausts is useful in the design and optimisation of the sound suppression systems.

The totality of the far-field sound from ducted exhausts is composed of the transmission of sound from the free supersonic jet (upstream of the duct inlet) to the far-field, the transmission of sound within the duct, and the radiation of sound from the duct exit and the subsonic jet (exiting the duct) to the far-field. Recent experiments on enclosed ducts by Kandula et al.[1-3] have indicated that the jet confinement has a significant effect on sound emission and directivity, suggesting that the duct modifies the sound generation and propagation.

According to Sir James Lighthill,[4,5] noise generation from subsonic jets is mainly due to turbulent mixing, and is comprised of the contributions of large-scale and fine-scale struc-

tures. The turbulent mixing noise is mainly broadband. In perfectly expanded supersonic jets (in which the nozzle exit pressure is equal to the ambient pressure), the large-scale mixing noise is manifested primarily as Mach wave radiation (Ffowcs Williams[6]; Tam[7]). The noise from Mach wave radiation is caused by the supersonic convection of large-scale turbulent eddies relative to the ambient fluid, and forms the dominant noise component. In imperfectly expanded (shock-containing) supersonic jets, additional noise is generated on account of broadband shock noise and screech tones.

A number of studies have been reported on enclosed subsonic flows typical of turbofan engine inlet/exhaust ducts[8,9] and mufflers for engine exhaust systems.[10] However, many of the theoretical studies on sound emission from turbulent supersonic jets are focused on unconfined (free) jets (Freund et al.[11]; Gamet and Estivalezes[12]; Kandula and Caimi[13]). There are very few reported studies on confined supersonic jets.[14] Reference[15] may be consulted for recent advances in aeroacoustics. The present study is concerned with experimental and theoretical simulation of the effect of the enclosing duct on the radiated noise from perfectly expanded cold supersonic jets. It summarises the effect of a rigid-walled exhaust duct in mitigating the sound from a supersonic cold nitrogen jet. In the present study the nozzle has an exit diameter of 25.4 mm, and is ideally expanded to an exit Mach number of 2.5. Predictions of the sound pressure levels are compared to the experimental data.[1-3]

2. DESCRIPTION OF THE EXPERIMENTAL PROGRAM

2.1. Nozzle and Duct Configuration

The test facility is outfitted with a chamber and a supersonic nozzle held in the vertical position. The chamber is fed from pressurised gaseous nitrogen bottles (8000 psi) in conjunction with two pressure regulators in series. The pneumatic system was modified to facilitate a continuous supply of nitrogen for the duration of the tests. Necessary instrumentation was provided for measurement of the acoustic and exhaust flowfields. The Mach 2.5 convergent-divergent nozzle was designed on the basis of the method of characteristics, and was made of stainless steel. The nozzle has an exit diameter of 25.4 mm, which compares with about a 1 m exit diameter typical of large rocket engines.

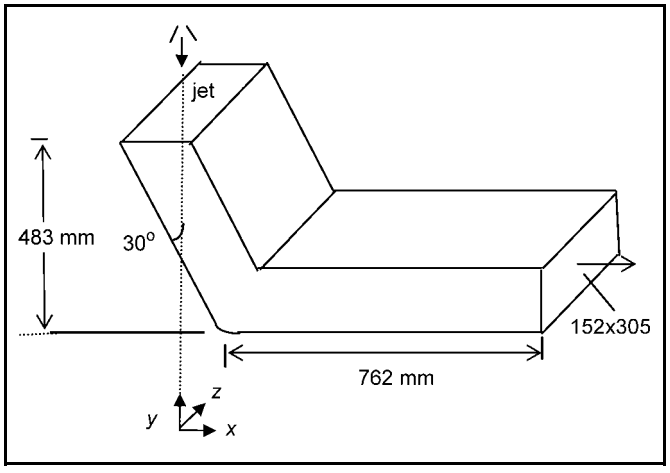

Figure 1. Geometry of the ducted exhaust jet configuration.

Figure 1 shows the geometry of the jet-duct configuration considered in the experimental data.[1-3] A scaled aluminum exhaust duct with an upstream J-deflector (30 degree inclination to the vertical) was fabricated and installed under the nozzle. The exit cross section of the duct is 152×305 mm. The exhaust duct can be positioned at desired levels relative to the nozzle exit plane (NEP). The origin of the coordinate system lies in the ground plane, with the y-axis coinciding with the jet axis. The jet impinges vertically on an upstream J-deflector (30 degrees to the vertical) of the duct before exiting horizontally through the duct. The nozzle exit is held fixed at 73 jet diameters (1.85 m) above the ground level. The duct inlet can be varied at 10, 5 and -1 jet diameters relative to the nozzle exit plane. The last position refers to the condition where the NEP is below the duct inlet.

Typical chamber and nozzle conditions for the scale-model test series considered here are given in Table 1. The Mach number of the exhaust jet was 2.5, and the jet Reynolds number was 58,300. The jet is perfectly expanded (nozzle exit pressure equals the ambient pressure p_∞ of 1.01×10^5 N/m^2). The ambient temperature was 294 K. The exit static temperature of the jet was 123 K, indicating that it is a cold jet, since the nozzle exit temperature is colder than the ambient temperature.

Table 1. Summary of nozzle parameters.

Parameter	Value
Stagnation pressure	1.72×10^6
Stagnation temperature, K	278
Nozzle mass flow rate, kg/s	0.77
Nozzle exit diameter, mm	25.4
Exit pressure, N/m^2	1.01×10^5
Exit temperature, K	123
Exit velocity, m/s	554.7
Nozzle exit Mach number	2.5
Jet exit Reynolds number	4×10^6

Photographic views of the free jet and the ducted jet testing with the Mach 2.5 cold nitrogen jet are presented in Figs. 2(a) and (b), respectively.

2.2. Flow and Acoustic Measurements

The chamber conditions (pressure and temperature) were measured by a pressure gauge and by a thermocouple mounted on the chamber wall. The exit Mach number was computed from the measurement of the total pressure and the static pressure at the NEP with the aid of a pitot tube equation[16] due to Lord Rayleigh. Brüel & Kjær microphones of 12.7 mm diameter were used for recording the sound pressure. The acoustic field surrounding the nozzle/duct configuration was measured with an array of acoustical transducers (microphones 1 through 9) placed azimuthally at 22.5-degree increments (Fig. 3). The sensors were placed azimuthally at 80 nozzle exit diameters from the NEP (thus representative of far-field conditions), and at a height of 54 jet diameters above the ground. The azimuthal array was setup in a plane parallel to the ground and centred on the jet axis. Also, the array was oriented at a polar angle of 76.6 degrees relative to the downstream axis at the nozzle exit. This angle is not in the peak noise radiation direction. This is about 50 degrees

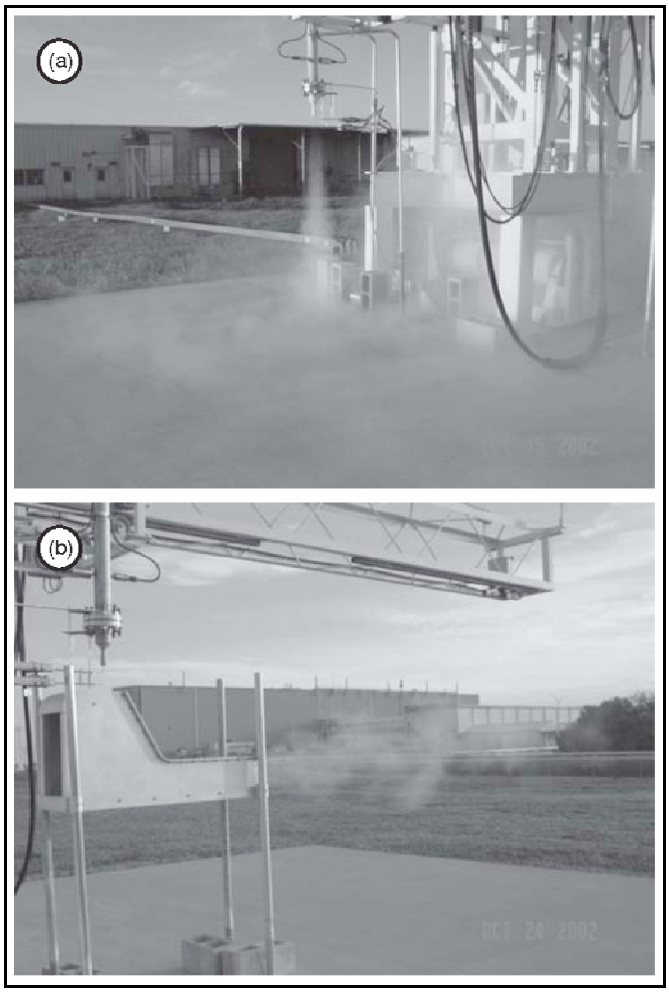

Figure 2. Photographs of the nitrogen supersonic (a) free jet and (b) jet flowing through an enclosed duct.

for free supersonic jets, which is typical of standard chemical rockets.[17] It should be pointed out that microphone 5 (at 0 degrees) is active only for the free jet, and is not active for the ducted jet case.

2.3. Data Acquisition

Time history measurements were made of chamber pressure, chamber temperature, and pitot and static pressures at the NEP. These measurements serve to indicate the time at which steady-state conditions are achieved. Generally, it takes about 60 s for steady conditions to prevail. As soon as the flow becomes steady, recording of acoustical data begins. Pressure-time data from the microphones were processed by the data acquisition system. The data were sampled at a rate of 125,000 samples/s so that sound frequencies up to 60 kHz could be recorded. The time domain data were processed in the form of narrowband spectra, octave-band sound pressure levels, and the overall sound pressure levels (OASPL) at each location, with the aid of LabVIEW software.

3. COMPUTATIONAL SIMULATION

The three-dimensional numerical simulation presented here is based on the computational fluid dynamics (CFD) work reported in reference[18]. In the CFD analysis, only the case of a ducted jet with $h = 254$ mm was considered. All computations were performed on an eight-processor SGI Origin 350 (700 MHz) machine.

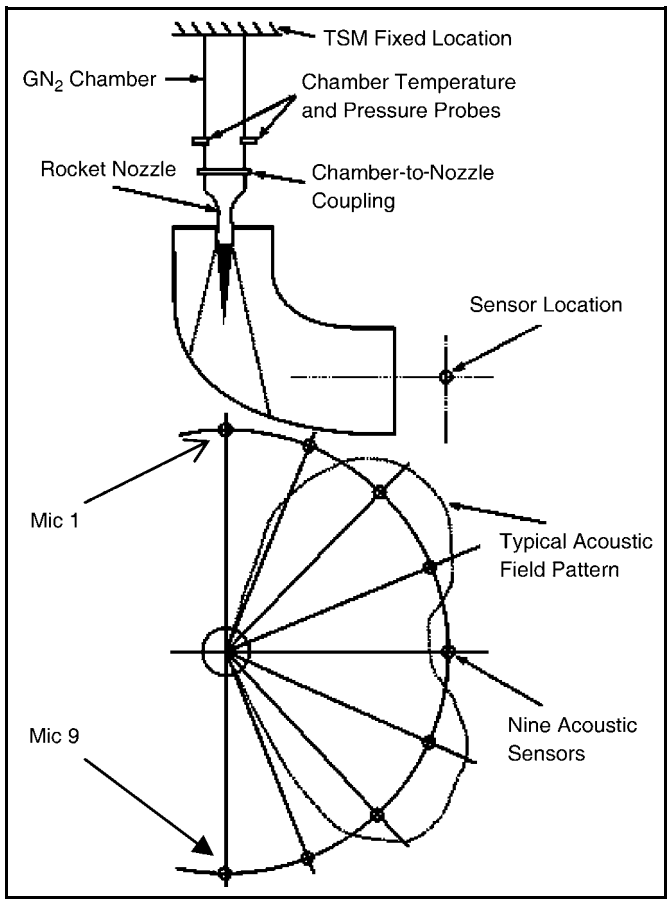

Figure 3. Sound pressure measurement setup.

3.1. Grid System

A side view of the grid system is presented in Fig. 4. The overall grid system consists of eight blocks with a total of about 4×10^6 grid points. Individual grids for the jet, duct, etc., were generated using the GRID-GEN grid generation program. In particular, the jet grid size was set at $75 \times 85 \times 58$ (axial, radial, and circumferential), and the duct grid size including the upstream flow-through part was $86 \times 50 \times 50$ (streamwise, and in the two cross section directions). The inter-grid communication was established by the Pegasus Code (Benek et al.[19]).

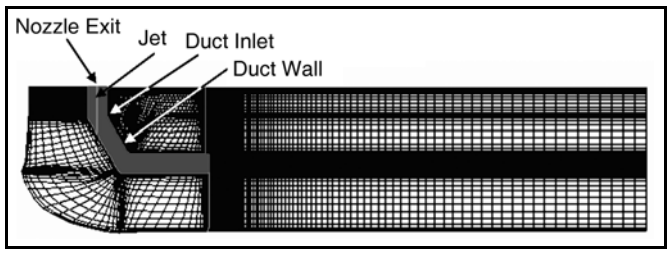

Figure 4. Grid system for the exhaust (side view).

For resolution purposes, grids were clustered in the regions of the jet shear layer, the duct wall region (interior and exterior), and the downstream section of the duct including its shear layer. Some typical dimensionless grid sizes (and distribution) scaled by the jet diameter are indicated as follows. For the jet grid, radial grid sizes were 0.01 near the axis, 0.0001 in the shear layer, and 0.09 for the outermost cell, while a uniform grid size of 0.3 was used in the axial direction. Referring to the duct grid, the first cell distance from

the wall was 0.01, and stretched to 0.35 near the centre. The grid size (transverse direction) in the shear layer downstream of the duct exit is maintained at 0.01. The first cell distance from the duct wall provides a value of y^+ of the order about 10. This suggests that the resolution is inadequate for resolving the viscous sublayer ($y^+ < 5$). Since the primary interest here was related to the pressure fluctuations in the boundary layer and not skin friction and heat transfer, and since the flow in the curved duct is not wholly a boundary layer type, it was believed that the relative coarseness of the duct grid would not appreciably affect the acoustical results.

3.2. Solution Procedure

The near-field solution for the mean flowfield and the acoustic field was obtained by the OVERFLOW CFD Navier-Stokes code (Kandula and Buning[20]). A multi-gridding scheme was chosen for accelerated convergence. The solution obtained is second-order accurate in space and time. The one-equation turbulence model of Spalart and Allmaras[21] was employed, which produces a solution for the turbulent kinetic energy. The Spalart-Allmaras turbulence model is used widely for external aerodynamics, and is known to be overly dissipative for separated flows, such as those present in the duct. Thus, it is likely that some error is encountered in the unsteadiness predicted by the code. A two-equation turbulence model such as the $k-\omega$ model[22] may be used to obtain improved accuracy. Initially the steady mean hydrodynamic flowfield is obtained by running the code with local time-stepping. A steady-state hydrodynamic flowfield solution (based on Reynolds time-averaged Navier-Stokes equations, RANS) was achieved within about 2000 iterations. Entrainment of the surrounding air into the jet becomes a part of the solution through the specification of freestream boundary conditions for the outer boundary.

Starting from the steady-state solution, a three-dimensional periodic disturbance was applied at the nozzle exit for exciting the shear layer as expressed by

$$u' = v' = w' = A\cos(\omega t)\exp\left[-\ln_2\left(\frac{s/r_j - h}{b}\right)^2\right], \quad (1)$$

where A denotes the amplitude of the disturbance, $\omega = 2\pi f$ is the angular frequency, r_j is the jet exit radius, and $s = \sqrt{y^2 + z^2}$ is the distance from the jet axis. The disturbance frequency f was based on a Strouhal number $St = 0.2$ (which was observed experimentally) corresponding to the most amplified large-scale instability waves (coherent structures) such as those of Kelvin-Helmholtz, which are responsible for Mach wave radiation. Exciting the jet at a single dominant frequency may not capture the true broadband character of the turbulent jet, and consideration of several frequencies (perhaps harmonics or random type) and of several modes (axisymmetric, helical etc.) is desired. The form of the exponential term (Gaussian profile) with $h = 0784$, and $b = 0.1$ was chosen here based on previous work on supersonic jet simulation.[13,18]

The predicted sound pressure level (SPL) is sensitive to the assumed levels of amplitude A, which depend on the nozzle flow conditions, and is unavailable in experimental data on jet noise. Generally speaking, the magnitude of the chosen amplitude of excitation must be sufficiently large to excite the shear layer (for instability waves), but at the same time it should be sufficiently small (weak) not to produce spurious acoustic waves. A value of $A = 0.01$ was considered for axisymmetric free jets.[12,13,23] Experience with axisymmetric supersonic jets by this author[13] has shown that a value of $A = 0.01$ predicts the observed peak radiation direction to within one degree, but underpredicts the measured peak OASPL by about 7 dB (in the peak radiation direction of 53 degrees and at 80 jet radii from the axis) for a Mach 2.0 free jet. Based on these considerations, the amplitude $A = 0.02$ is considered in the present investigation. It may be remarked that for modelling of imperfectly expanded supersonic jets, there is no need to prescribe the excitation at the nozzle exit.

For the acoustic solution, appropriate time-dependent boundary conditions were applied to minimise reflections from the finite computational boundaries. Thompson's outflow acoustic boundary condition (Thompson[24]) was applied at the outflow boundary (downstream end of the grid), which maintains the mean static pressure at the ambient level. The acoustic radiation boundary condition of Tam and Webb[25] was assumed for the lateral boundaries. At the supersonic inflow, all data are specified, such that all time variations of the characteristic variables are set to zero because all waves are incoming waves. These boundary conditions have been implemented by the author in the OVERFLOW code.[13] The code was run time-accurately for about 22000 iterations to ensure that a periodic state is approached.

In the far-field, the sound pressure levels were determined by the Kirchhoff formulation (Kirchhoff[26]) with data on the Kirchhoff surface obtained by the CFD code. The method is presented in Lyrintzis and Mankbadi[27], and has been considered by the author for an axisymmetric supersonic jet simulation (Kandula and Caimi[13]). The data on the Kirchhoff surface (enclosing the nonlinear source region) include the time history of pressure, normal pressure derivative, and pressure-time derivative. It is known that the Kirchhoff method can yield poor results if there is significant vortical flow passing through the surface (Brentner and Farassat[28]). The Kirchhoff solver is linear in the far-field (outside the Kirchhoff surface). Thus proper care needs to be exercised in choosing the locations of the Kirchhoff surface, so that the predicted far-field SPL is not dependent on its location. For free supersonic jets, six jet radii for the location of the Kirchhoff surface are recommended.[12,13,27] In the present simulations, the Kirchhoff surface for each grid was taken to be about seven grid cells from the outer boundary, at which the computed results were found to be satisfactory.

4. RESULTS AND COMPARISON

4.1. Spectral Sound Pressure Level

The spectral content of the octave sound pressure level (SPL) for the free jet and the closed-duct cases is shown in Figs. 5(a) and (b), respectively. A peak frequency of about 4 kHz is noted in this case and agrees well with the estimated value based on a Strouhal number ($St = fu_j/d_j$) of 0.2. Here f denotes the frequency, u_j is the nozzle exit velocity, and d_j is the nozzle exit diameter. The free jet shows some asymmetry in the spectra (2 to 5 dB) in the high frequency range of 4-8 kHz, which is perhaps due to the nonanechoic character

of the experimental facility and to the presence of the neighbouring structures. The relatively rapid decay in the measured SPL at 12.5 kHz is due to the fact that the present sensors are designed for a maximum frequency of 20 kHz. The measured SPL spectrum for the free jet is seen to be consistent with widely used correlations given in NASA-SP method.[17] Good agreement is noted for the peak frequency. The OAPSL obtained from using the NASA-SP method is 125.0 dB, which compares with the present measurement of 129.5 dB.

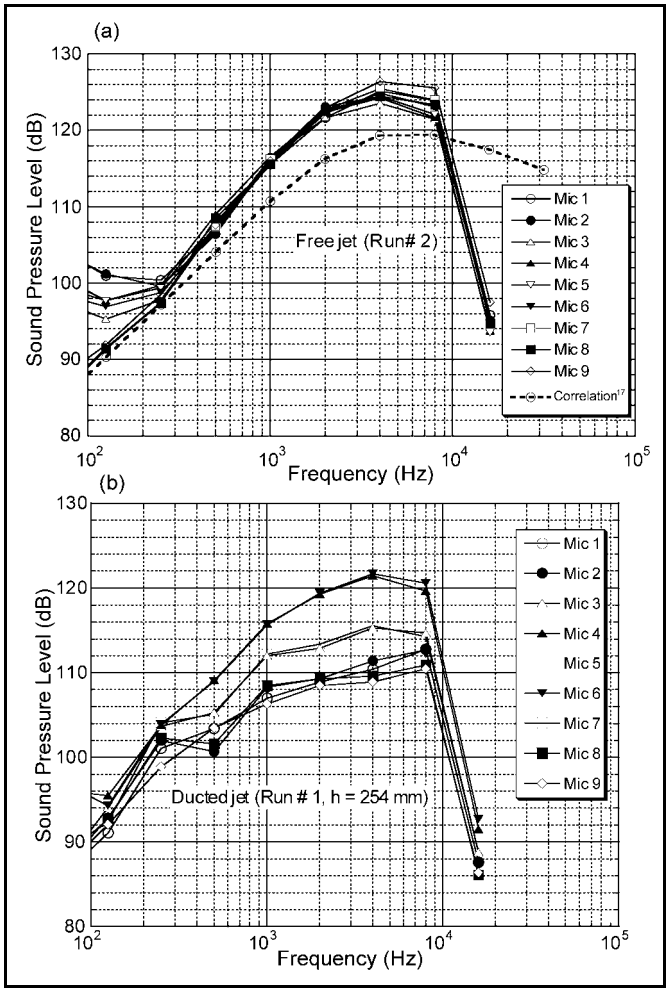

Figure 5. Spectral sound pressure levels for (a) the free jet and (b) for the jet flowing in a duct.

In the ducted jet case, the peak frequency near $\theta = 0$ degrees (corresponding to the duct axis) is about 4 kHz, which is close to the free-jet value. However, the peak frequency increases as the angle from the jet axis is increased. Differences in the spectrum for various angles are observed over a wide range of frequencies (roughly 1.5 decades).

4.2. Overall Sound Pressure Level (OASPL)

Figure 6 shows a comparison of the OASPL for the free jet with those obtained for a jet passing through a duct, with the NEP located at different heights relative to the duct inlet. This figure shows the sound directivity in the ducted jet system[1-3] with data taken along a 2.03 m arc radius about the jet axis, and in a horizontal plane 1.37 m above the ground level. The quantity *h* refers to the height of the nozzle exit plane above the duct inlet plane. The directivity for the free jet is in a single plane perpendicular to the free jet axis and is thus axisymmetric. While there is axial symmetry in the OASPL for the free jet, there is considerable directivity in the OASPL in the presence of the exhaust duct. The measured directivity pattern for the ducted jet corresponds to a slower jet (with entrained mass flow) rotated 90 degrees to the original free jet axis. It thus resembles typical jet directivity in a single plane, but now the angle is with respect to the horizontal ducted jet axis.

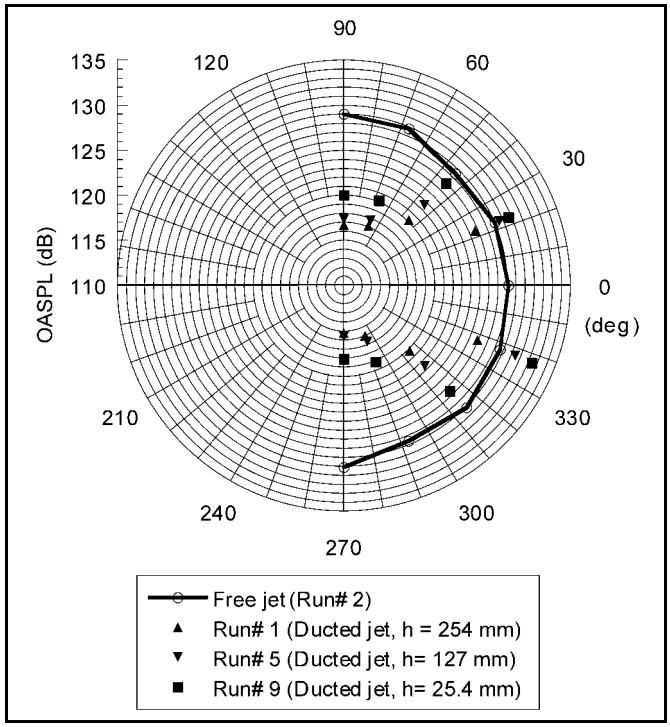

Figure 6. Effect of nozzle height on the directivity of sound radiation for a ducted jet.

When the NEP is held at 254 mm above the duct inlet, a reduction in the maximum OASPL of about 3 dB (near the ducted jet axis) is achieved relative to the free jet case. Relatively large reductions in OASPL are noted at ±90 degrees. These findings suggest that there is an optimum location of the NEP relative to the duct inlet plane, which results in the largest reduction in the OASPL.

4.3. CFD/Kirchhoff Solution

Air entrainment. CFD calculations (for $h = 254$ mm) show that there is significant entrainment of air into the duct. It is seen that the entrained air flow is about 3.2 times the mass flow rate of jet exit. This result is representative of entrainment in practical exhaust duct configurations.

Instantaneous flowfield. Figure 7 displays the instantaneous Mach number contours in the duct and in the region downstream of the duct exit at a lateral location near the axis of the duct. While the jet exit Mach number is 2.5, the flow at the duct exit is subsonic around Mach 0.45.

Acoustic pressure. The acoustic pressure (obtained by subtracting the mean pressure from the instantaneous pressure) for the jet-duct system is illustrated in Fig. 8(a). The directivity of the Mach wave radiation from the initially supersonic jet (unenclosed portion) is seen. The plot also shows the diffraction pattern of sound around the duct. Figure 8(b) shows an expanded view of the sound pressures within the

duct, showing the sound reflections and propagation within the duct. It also reveals the sound pressure contours in the jet, showing the three-dimensional character of the disturbance in the jet. Calculations show that the OASPL at the location of the jet impingement within the duct is of the order of about 180 dB.

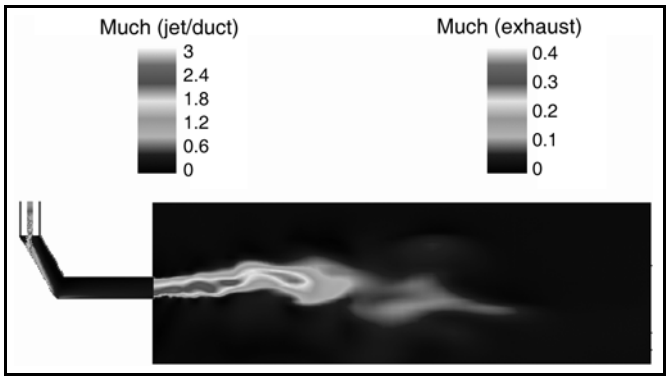

Figure 7. Instantaneous Mach number contours in the exhaust jet.

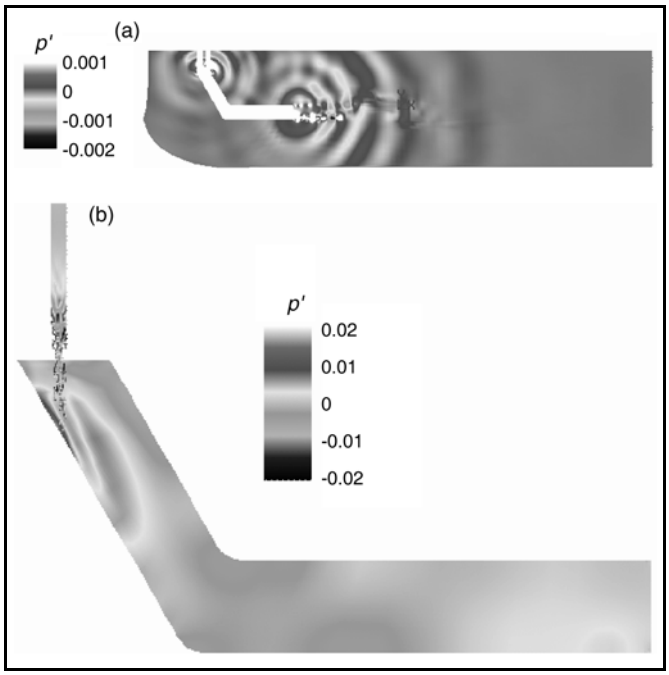

Figure 8. Sound pressure contours (a) in the jet-duct system (excluding the duct) and (b) in the duct region.

4.4. Comparison of Theory with Experimental Data

The acoustic far-field computations of sound pressure levels are based on the Kirchhoff surface integral. Figure 9 presents a comparison of the predictions of the directivity of the OASPL with the test data[1-3] for a ducted jet. The OASPL data are presented as a function of the azimuthal angle measured from the axis normal to the duct exit plane. While the free jet data for the OASPL show symmetry, the OAPSL for the closed duct shows considerable directivity, with the OASPL decreasing with the increasing angle. Satisfactory agreement is noted between the theory and the data. The theory predicts the OASPL with an accuracy of about 2 dB. At the 0 degrees position, the predicted OASPL is considerably lower than that of the free jet due perhaps to the effect of refraction. The OASPL data at 0 degrees was not available for the ducted jet case because the free-field microphone could not be installed there due to the possibility of damage. The results and comparisons will be useful in the development of scaling laws for ducted jet noise, such as those considered for free jets (McInerny[26], Kandula and Vu[27]).

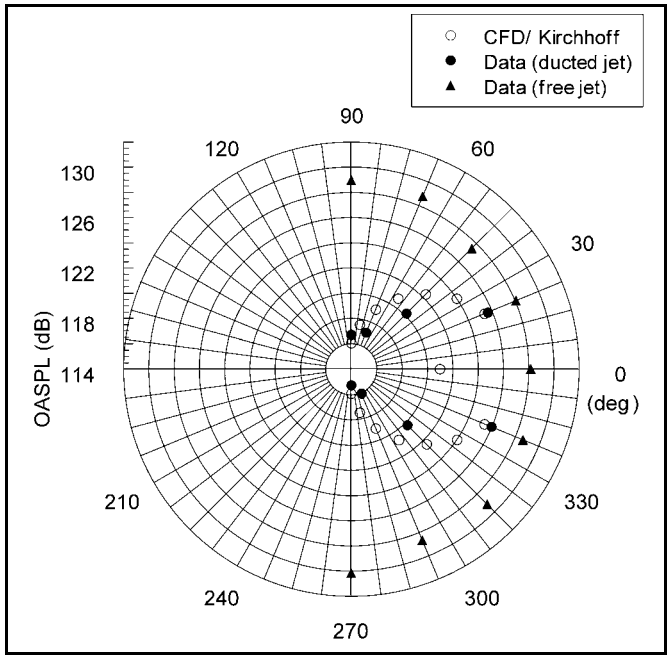

Figure 9. Comparison of the directivity of the overall sound pressure level.

Because of the storage problem associated with the computing system employed, the spectral content of the predicted radiated noise could not be extracted. The seemingly close agreement in the absolute values of OASPL between the theory and the data should be observed with caution in view of the approximations and limitations inherent in the modelling. Comparisons of the SPL spectra and the OASPL at several polar angles are recommended for further validation of the numerical model.

5. CONCLUSIONS

With the use of an exhaust duct containing an upstream J-deflector, the measured maximum overall sound pressure level of a Mach 2.5 supersonic jet is reduced by about 3 dB. The measurements only suggest that the OASPL is reduced in one plane at the particular polar angle considered. The observed peak frequency is found to increase above the free-jet value as the angle from the jet axis is increased. The results also suggest that there is an optimum distance between the nozzle exit plane and the duct inlet for minimising the sound pressure. With increased duct lengths and absorbing liners, larger reductions in sound pressure level may be realised. Numerical simulation of sound for the ducted jet configuration has also been carried out. Entrainment of air into the duct, of the order of three times the jet mass flow rate, was noted. The presence of the duct significantly modifies the character of the far-field directivity of the overall sound power level. Satisfactory agreement is noted between the theory and the measurements for the far-field directivity. The method has potential for the investigation of hot imperfectly expanded jets in lined ducts with application to actual rocket exhausts.

Acknowledgement

The authors would like to thank Wayne Crawford, Geoffrey Rowe, Jeffrey Crisafulli, and Charles Baker of the Launch Equipment Test Facility (LETF) at NASA Kennedy Space Center for their assistance in various aspects of the test program. This work was funded by Air Force Research Laboratories (AFRL), Wright-Patterson Air Force Base, Ohio, with Gregory Moster as Technical Monitor. This work is also partially supported by funding from the Kennedy Space Center Director Discretionary Fund (CDDF). Thanks are also due to Prof. Tasos Lyrintzis of Purdue University for kindly providing the YORICK Kirchhoff code. The valuable suggestions and criticism of the reviewers are gratefully acknowledged. Papers by the author from 1973 to 1982 were published with the name 'K. Mastanaiah.'

REFERENCES

[1] Kandula, M. and Vu, B. Scale model experiments on sound propagation from a Mach 2.5 cold nitrogen jet flowing through a rigid-walled duct with a J-deflector, NASA TM-2003-211186, Kennedy Space Center, (2003).

[2] Kandula, M., Margasahayam, R., and Vu, B. Sound propagation from a supersonic jet flowing through a rigid-walled duct with a J-deflector, *Proceedings of the 10th International Congress on Sound and Vibration*, Stockholm, Sweden, **4**, 2253-2260, (2003).

[3] Vu, B. and Kandula, M. Noise mitigation of ducted supersonic jets for launch exhaust management systems, *JANNAF 27th Plume Technology Subcommittee Meeting*, NASA Stennis Space Center, Bay St. Louis, Mississippi, (2003).

[4] Lighthill, M. J. On sound generated aerodynamically, I. General theory, *Proc. Roy. Soc. A*, **211**, 564-587, (1952).

[5] Lighthill, M. J. On sound generated aerodynamically, II. Turbulence as a source of sound, *Proc. Roy. Soc. A*, **222**, 1-32, (1954).

[6] Ffowcs Williams, J. E. The noise from turbulence convected at high speed, *Proc. Roy. Soc. A*, **255**, 469, (1963).

[7] Tam, C. K. W. On the noise of a nearly ideally expanded supersonic jet, *J. of Fluid Mechanics*, **51**, 69-95, (1972).

[8] Eversman, W. and Roy, I. D. Ducted fan acoustic radiation including the effects of nonuniform mean flow and acoustic treatment, AIAA-93-4424, (1993).

[9] Ozyoruk, Y. and Long, L. Computation of sound radiated from engine inlets, *AIAA Journal*, **34**, 894-901, (1996).

[10] Hota, R. N. and Munjal, M. L. A new hybrid approach for the thermo-acoustic modelling of engine exhaust systems, *International Journal of Acoustics and Vibration*, **9** (3), 129-138, (2004).

[11] Freund, J. B., Lele, S. K., and Moin, P. Numerical simulation of a Mach 1.92 turbulent jet and sound field, *AIAA Journal*, **38**, 2023-2031, (2000).

[12] Gamet, L. and Estivalezes, J. L. Application of large-eddy simulations and Kirchhoff method to jet noise prediction, *AIAA Journal*, **36**, 2170-2178, (1998).

[13] Kandula, M. and Caimi, R. Simulation of jet noise with OVERFLOW CFD code and Kirchhoff surface integral, AIAA-2002-2602, *8th AIAA/CEAS Aeroacoustics Conference*, Breckenridge, Colorado, (2002).

[14] Khan, Md. T. I., Seto, K., Xu, Z., and Takeshi, M. Aero-acoustic performance of a tube with forward-slanted oblique perforations for reducing the noise of a supersonic jet, *International Journal of Acoustics and Vibration*, **9** (1), 23-29, (2004).

[15] Campos, L. M. B. C. On some recent advances in aeroacoustics, *International Journal of Acoustics and Vibration*, **11** (1), 27-45, (2006).

[16] Shapiro, A. H. *The Dynamics and thermodynamics of compressible fluid flow*, Vol. 1, Wiley, New York, (1953).

[17] Eldred, K. M. Acoustic loads generated by the rocket propulsion system, NASA-SP-8072, (1971).

[18] Kandula, M. Numerical simulation of noise from a supersonic jet passing through a rigid duct, AIAA-2004-2935, *10th AIAA/CEAS Aeroacoustics Conference*, Manchester, Great Britain, (2004).

[19] Benek, J. A., Buning, P. G., and Steger, J. L. A 3-D grid embedding technique, AIAA-85-1523-CP, (1985).

[20] Kandula, M., and Buning, P. G. Implementation of LU-SGS algorithm and Roe upwinding scheme in OVERFLOW thin-layer Navier-Stokes code, AIAA-94-2357, (1994).

[21] Spalart, P. R. and Allmaras, S. R. A one-equation turbulence model for aerodynamic flows, AIAA-92-0439, (1992).

[22] Kandula, M. and Wilcox, D. C. An examination of turbulence model for boundary layers, free shear layers and separated flows, AIAA-95-2317, *26th AIAA Fluid Dynamics Conference*, San Diego, CA, (1995).

[23] Mankbadi, R., Hixon, H., and Shih, S. H. Use of linearized Euler equations for supersonic jet noise prediction, *AIAA Journal*, **36**, 140-147, (1998).

[24] Thompson, K. W. Time-dependent boundary conditions for hyperbolic systems I, *Journal of Computa-tional Physics*, **89**, 439-461, (1990).

[25] Tam, C. K. W. and Webb, J. C. Dispersion relation-preserving finite difference schemes for computational aeroacoustics, *Journal of Computational Physics*, **107**, 262-281, (1993).

[26] Kirchhoff, G. R. Zur Theorie der Lichtstrahlen, *Annalen der Physik und Chermie*, **18**, 663-695, (1883).

[27] Lyrintzis, A. S. and Mankbadi, R. R. Prediction of the far-field jet noise using Kirchhoff's formulation, *AIAA Journal*, **32**, 413-416, (1996).

[28] Brentner, K. S. and Farassat, F. Analytical comparison of acoustic analogy and Kirchhoff formulation for moving surfaces, *AIAA Journal*, **36**, 1379-1386, (1999).

[29] McInerny, S. Rocket noise - a review, AIAA Paper 90-3981, *13th Aeroacoustics Conference*, (1990).

[30] Kandula, M. and Vu, B. On the scaling laws for jet noise in subsonic and supersonic flow, AIAA-2003-3288, *9th AIAA Aeroacoustics Conference*, Hilton Head, South Carolina, (2003).